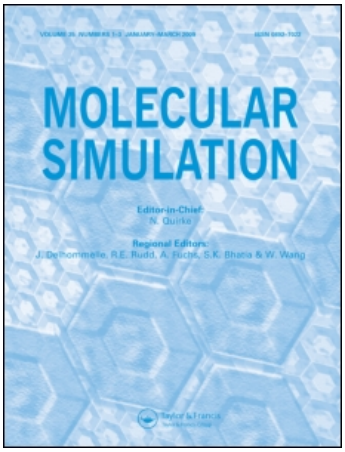

Molecular Simulation
Publication details, including instructions for authors and subscription information:
http://www.informaworld.com/smpp/title~content=t713644482

The Microcrystal Melting Transition

N. Quirke[a]
[a] BP Research Centre, Sunbury on Thames, UK

To cite this Article Quirke, N.(1988) 'The Microcrystal Melting Transition', Molecular Simulation, 1: 4, 249 — 270
To link to this Article: DOI: 10.1080/08927028808080947
URL: http://dx.doi.org/10.1080/08927028808080947

Molecular Simulation, 1988, Vol. 1, pp. 249–270
Photocopying permitted by license only
Reprints available directly from the publisher

THE MICROCRYSTAL MELTING TRANSITION

N. QUIRKE

BP Research Centre, Chertsey Road, Sunbury on Thames, UK

(*Received Oct 1987*)

Metropolis Monte Carlo simulations of the melting transition of Lennard-Jones microcrystals confined to spherical cavities are reported. While 13 atom microcrystals melt continuously, larger microcrystals containing 201 and 209 atoms exhibit a first-order-like freezing transition to an HCP structure. A simple formula is derived which predicts the marked lowering of the melting temperature for small microcrystals observed in the simulations and which is consistent with experimental results for the melting of metal microcrystals. The Tammann temperature is found to be an accurate indicator of microcrystal melting.

KEY WORDS: Finite-size effects, melting, microcrystals, Tammann temperature

1. INTRODUCTION

The variation of thermodynamic, structural and other properties of materials as a function of system size is of importance in many areas of science and technology. Small systems play a crucial role in nucleation [1], crystal growth [2], catalysis [3], adsorption [4], radiation damage [5] and increasingly in new materials and devices [6]. Much work has been done on finite size effects for spin systems [7, 8] where the change in, for example, critical temperatures with system size and boundary conditions are now well understood. However, a detailed understanding of finite size effects on melting in real materials requires that factors such as positional disorder and many-neighbour interactions be considered. This is more naturally accomplished using particle models. In recent years, the Lennard-Jones potential has been employed in simulation studies of microcrystals under various external constraints [9–15], and it is now clear that microcrystal structures are not necessarily those of the bulk material, and that melting takes place between an ordered microcrystalline phase and an inhomogeneous liquid phase (if constrained by cavity walls) at temperatures considerably lower than the bulk melting temperature. There is, however, still some uncertainty as to the details of the approach to bulk behaviour and the nature of the microcrystalline melting transition.

A comparison of the microcrystal melting transition with the bulk phenomenon is facilitated by imposing a constraint on the volume of the system. This prevents evaporation and may be arranged to have little effect on the solid phase or the melting temperature – as a consequence, long simulation runs are possible with a fixed number of atoms. In the present work, a spherical constraint has been imposed on the clusters of atoms such that the liquid phase has a mean density comparable to that of the bulk liquid phase near the triple point. Very large numbers of configurations ($\sim 60 \times 10^6$) have been generated to avoid metastable states and reduce the statistical errors. The

simulation of a cluster inside a constraining cavity may be considered as an idealised model of the situation of metal clusters in zeolite cages.

In a previous letter [12] the results of a preliminary investigation of the melting transition of 13 atom Lennard-Jones clusters constrained to a spherical cavity using Metropolis Monte Carlo simulation were reported. Melting was shown to take place at approximately half the bulk melting temperature via a continuous transition from an icosahedral microcrystalline structure to an inhomogeneous liquid phase. A three-body correlation function was introduced and shown to be useful in monitoring the melting transition. It was demonstrated that the "solid-liquid" transition of Kaelberer and Etters [10] for 13 atoms in a vacuum was associated with premelting phenomena and not with a sharp melting transition. It should be noted that if vacuum clusters are simulated for long enough they eventually evaporate. The rate of evaporation is controlled in a Metropolis Monte Carlo simulation by the maximum displacement parameter. Berry et al [13–15] have published detailed studies of 13 atom clusters in vacuum and have suggested that for a range of temperatures in the "melting region" of the metastable cluster they can be considered to be a mixture of "solid" and "liquid" configurations. In the light of this work and the new results to be presented here, the Kaelberer and Etters "transition" appears to mark the temperature at which significantly disordered configurations first appear in the low temperature ensemble. However, the clusters are still predominantly solid-like for a range of temperatures above this point.

In the present work the problem of metastability in vacuum is avoided by considering 13, 201 and 209 atom clusters *confined to cavities*. The larger clusters provide valuable information on the manner in which microcrystal properties approach those of the bulk phase as the number of particles increases. A very slow approach to bulk behaviour is observed for the melting temperature. However, the melting transition itself rapidly becomes bulk-like. By considering microcrystal surface free energies, expressions have been derived which predict the variation of the microcrystal melting temperature with size. In what follows, quantities are reduced by the usual Lennard-Jones parameters ε, σ as follows, $T^* = k_B T/\varepsilon$, T = temperature, $\rho^* = N/V\,\sigma^3$, N = number of atoms, V = cavity volume, $U^* = U/N\varepsilon$, U = configurational energy, $C_v^* = C_v/Nk_B T$, C_v = configurational specific heat, $r^* = r/\sigma$ r = atom-atom separation.

2. THE NATURE OF MICROCRYSTAL MELTING

In this section the results of extensive Metropolis Monte Carlo simulations on clusters of Lennard-Jones atoms are described. Simulation details may be found in an appendix. Section 2.1 reports the thermodynamic properties of the microcrystals as they melt. Section 2.2 describes the microcrystalline structure observed in the simulations and its change on melting. In section 2.3 an expression for the microcrystal melting temperature is obtained and used to describe the approach to the bulk melting temperature.

2.1 Melting Curves

In this section plots of the configurational energy for $N = 13$, $N = 201$ and $N = 209$ atom microcrystals confined to spherical cavities of mean density $\rho^* = 0.875$ are

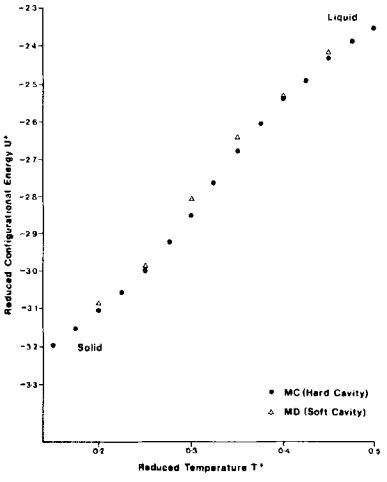

Figure 1A The variation of configurational energy with temperature for a 13 atom cluster of Lennard-Jones atoms under various constraints. ● Metropolis Monte Carlo simulations in the canonical ensemble (MC) with a hard spherical cavity boundary. Δ, molecular dynamics simulation at constant temperature (MD) in a soft cavity.

presented (the volume of the cavity has been taken to be the volume containing the atomic centres). The variation of thermodynamic properties with temperature can be used to determine the melting temperature, and to show the change in the melting process as the number of particles increases.

In Figure 1A the variation of the configurational energy with temperature is plotted for a 13 atom cluster as it changes from an icosahedral microcrystalline solid to an inhomogeneous liquid. Two sets of results are shown for different simulation methods and cavities. The details of the cavity wall–atom potentials are given in an appendix. Metropolis Monte Carlo simulations of the 13 atom cluster in a hard cavity produce a curve with a linear dependence on T^* at low and high temperatures and an intermediate region connecting them. Two and three body correlation functions measured in the clusters (discussed below) allow an identification of the low temperature clusters as solid and high temperature clusters as liquid phases. The melting is reversible on cooling with no supercooling apparent for the present length of simulation run (see appendix). Molecular dynamics simulations of the same system in the isokinetic ensemble but with a soft cavity wall produce similar results, as can be seen in Figure 1A.

Figure 1B shows the configurational specific heat (calculated from fluctuation properties) as a function of temperature for the Metropolis Monte Carlo simulations of the 13 atom cluster confined to a hard cavity. A peak is visible near $T^* = 0.3$ corresponding to the centre of the curved region of Figure 1A. Inspection of the cluster structure at temperatures on either side of the peak indicates that to the left of the peak the *average* structure is solid-like and that to the right it is liquid-like. The temperature at which the peak in specific heat occurs has been taken as the melting temperature although, due to the continuous nature of the transition and the statistical errors in the simulation, this identification can only be approximate. (Detailed tables of results relating to the 13 atom clusters are to be found in the appendix). The

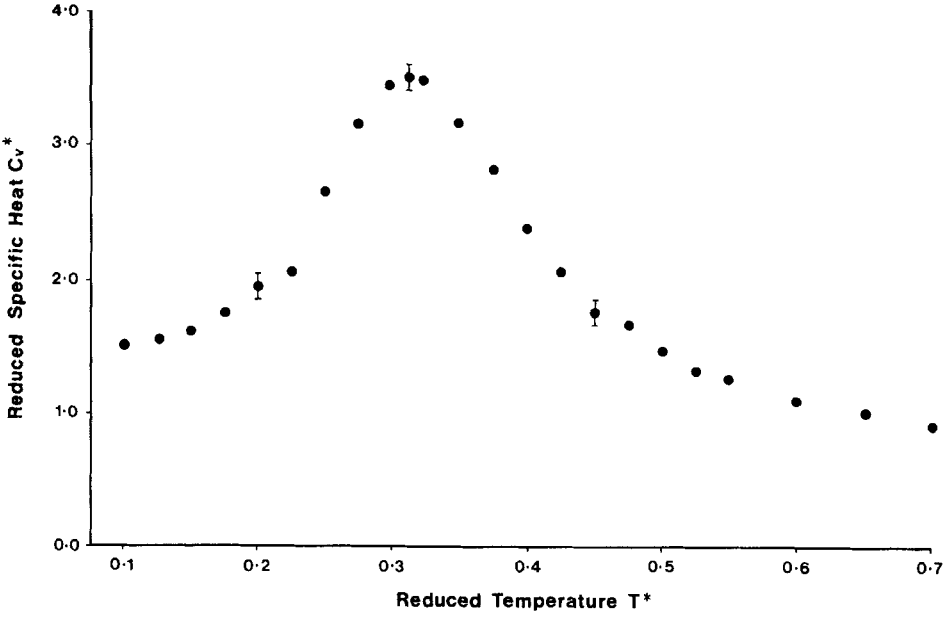

Figure 1B The configurational specific heat for the MC simulations of *Figure* 1A as a function of temperature.

peak in the specific heat is at $T^* = 0.3125 \pm 0.025$ and may be taken as the reduced melting temperature of the 13 atom cluster $T_m^*\{13\}$. This should be compared to the bulk triple point temperature for the Lennard-Jones system of $T_{TP}^* = 0.68 \pm 0.02$ [20]. The 13 atom melting transition appears to be quite smooth within the resolution of these calculations with neither $U^*(T^*)$ nor $C_v^*(T^*)$ displaying sharp discontinuities and seems not to depend on the details of the atom-cavity wall potential.

A distribution function giving the probability density of finding configurations with potential energies between U^* and $U^* + dU^*$ for 13 atom clusters at several temperatures is shown in Figure 1C for the hard cavity. At high and low temperatures on either side of the specific heat peak of Figure 1B the distributions are symmetric while in the melting region a pronounced asymmetry develops although no double peaks such as those reported by Berry et al [13–15] for clusters in vacuum are discernible. However, there is considerable overlap between these functions at high and low temperatures which, as is shown in the next section, is the result of the mixing of ordered and disordered configurations in the equilibrium ensemble. This behaviour which has also been seen in small clusters by Berry et al [13–15] who interpreted it in terms of a model with two transition (melting and freezing) temperatures is a consequence of the finite size broadening of the first order bulk melting transition. Challa et al have demonstrated similar mixing in the 10 state Potts model [8].

The melting transition for the 201 atom cluster is apparent in the plot of energy against temperature shown in Figure 2A. The transition between the solid and liquid phases is now much sharper. The results displayed in Figure 2A and Table A2 were obtained by slow cooling from a 201 atom configuration cut from a bulk liquid

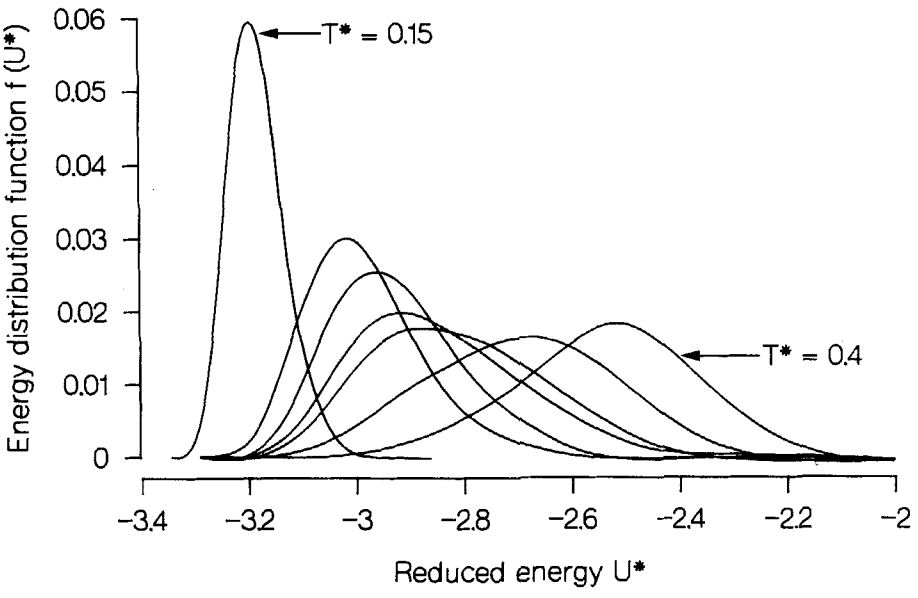

Figure 1C Energy distribution functions for 13 atom clusters confined to spherical cavities. Taking curves from left to right (refer to peaks) the temperatures are $T^* = 0.15, 0.25, 0.275, 0.3, 0.3125, 0.35, 0.4$. No double peaks are apparent, but high temperature ensembles ("liquid") sample very low energy (very ordered) configurations.

simulation at $\rho^* = 0.875$ and $T^* = 10$. Similar results were produced with different initial conditions. Freezing has been taken to occur at $T_m^*\{201\} = 0.3725 \pm 0.0025$, the "latent heat" of the transition is approximately $\Delta U^* = 0.18$.

Figure 2B shows the freezing transition for a 209 atom cluster. This cluster behaves in a similar fashion to the 201 atom cluster; the measured freezing temperature is $T_m^*\{209\} = 0.385 \pm 0.005$. The "latent heat" of the transition is approximately $\Delta U^* = 0.24$, slightly larger than that for 201 atoms.

From the $N = 201$ and 209 atom cluster results presented in Figure 2, it is clear that although the melting temperature is still very low, the melting transition is much closer in character to bulk melting than for the 13 atom cluster. A sharp change in the configuration energy is observed for the larger clusters at the melting temperature. These results are consistent with previous theoretical work [40] which has suggested $N = 200$ as a characteristic value of N for the onset of bulk first-order melting properties.

2.2 Cluster Structure

In the last section the presence of a melting transition was inferred from the behaviour of the thermodynamic properties of clusters. In this section the average structures in the microcrystalline and liquid phases for clusters of 13, 201 and 209 atoms are described.

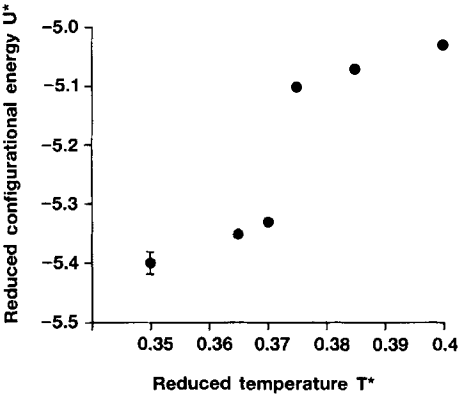

Figure 2A The cooling curve of the 201 atom cluster.

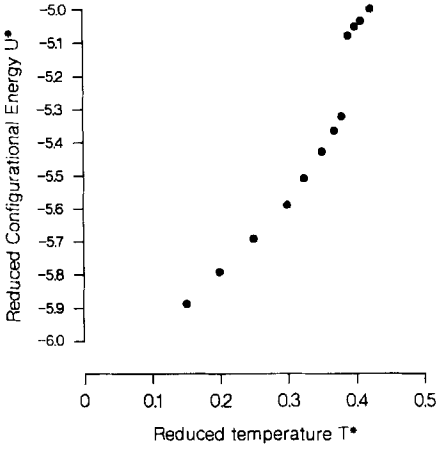

Figure 2B The cooling curve for the 209 atom cluster.

2.2.1 The 13 atom cluster

The 0K minimum energy configuration of the 13 atom cluster is an icosahedral microcrystal [21]. Previous workers [9–12] have shown that the icosahedral structure is stable at finite temperatures below the microcrystal melting temperature and therefore presumably has the lowest free energy at low temperatures. The presence of icosahedral ordering can be inferred from two body correlation functions (taken over the whole cluster) such as the radial distribution function $g(r^*)$. For example, in the present work, the starting configuration of a 13 atom cluster simulation has been taken to be the face centred cubic (FCC) microcrystal. For this close packed structure $g(r^*)$ has a peak at $r^* = 1.6$ representing second nearest neighbours. As the system approaches the equilibrium icosahedral form this peak disappears. At very low temperatures ($T^* < 0.025$) the first peak in $g(r^*)$ splits reflecting the difference in near neighbour separations between atoms entirely in the surface and the distance between the central atom and the surface atoms in a perfect icosahedron [21].

Figure 3A shows the radial distribution function for three temperatures spanning the melting transition of Figure 1 calculated by averaging over all pairs in clusters confined to a hard cavity, (note that in contrast to radial distribution functions for bulk phases this tends to zero at large r^* as there are no pairs with a separation greater than the cavity diameter). For the lowest temperature displayed ($T^* = 0.225$) there are peaks at $r^* = 1.1$, 1.9 and 2.2. As discussed above these peaks are consistent with icosahedral ordering. A region of very low probability exists between the first and second peaks, indicating a well defined microcrystalline structure. As the temperature is raised, a gradual smoothing of the peaks and troughs takes place associated with a gradual loss of average atom–atom ordering. By $T^* = 0.4$ all trace of the peak at $r^* = 2.2$ has gone and the trough at $r^* = 1.6$ has filled considerably. The radial distribution function for $T^* = 0.475$ (not shown) is not materially different from that for $T^* = 0.4$. Figure 3B shows the function $C(R^*)$, the wall–atom radial distribution function of the cavity for the same temperatures as Figure 3A. As in Figure 3A, small differences mark the transition from icosahedral ordering to a more disordered state. There is a gradual build up of atoms at the cavity wall (corresponding to an increased

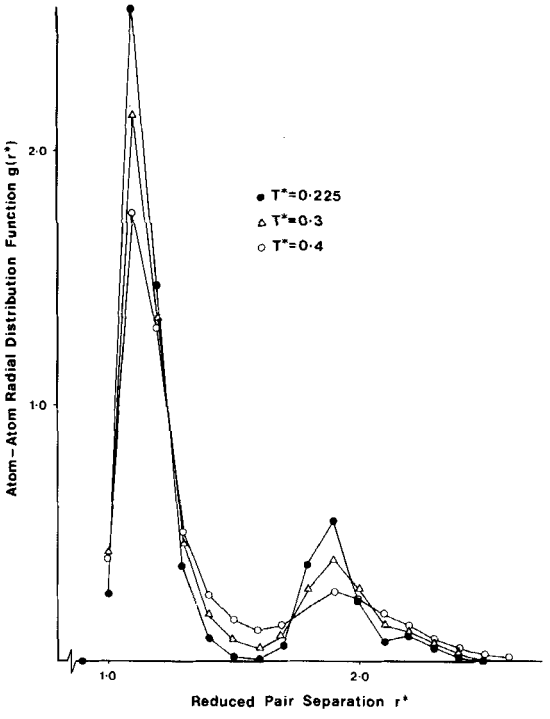

Figure 3A Radial distribution functions for the 13 atom cluster. These structures correspond to the MC configurational energies given in *Figure* 1A.

normal pressure), and a filling in of the trough at $R^* = 0.9$, although the higher temperature clusters remain inhomogeneous.

A clearer picture of how the 13 atom cluster ordering has changed between the "solid" and "liquid" phases emerges from Figure 3C. In this figure the function $f(\cos\theta)$, the fraction of interior angles of triplets of atoms, with pair separations up to $R^*_{max} = 1.35$, having a cosine between $\cos\theta$ and $\cos\theta + d\cos\theta$, is plotted against $\cos\theta$ for $T^* = 0.225$, 0.3 and 0.4. This function can be used to discriminate between different solid structures at low temperatures since it describes the nearest neighbour anisotropy. For example, the perfect face centred cubic (FCC) lattice has peaks in $f(\cos\theta)$ at -1, ± 0.5, 0.0, the hexagonal close packed (HCP) lattice has peaks at -1, -0.83, ± 0.5, -0.33, and 0.0 while the icosahedral structure has peaks near -1, ± 0.5. At finite temperatures the peaks are broadened but still discernable with regions of low probability in between. The results for $T^* = 0.225$ in Figure 3C show the microcrystal to have a temperature broadened icosahedral structure (this is confirmed by a visual inspection of the particle configurations). There are strong peaks near -1, ± 0.5, with regions of very low probability near -0.8 and 0.0. As the temperature is raised the peaks decrease in height and become broader although at $T^* = 0.3$ the nearest neighbour structure still seems quite ordered (however, there are significant defects as can be seen from the finite probability of 90° angles ($\cos\theta = 0$) for this temperature). At $T^* = 0.4$ the peak at -1 has gone and apart from peaks at 0.5

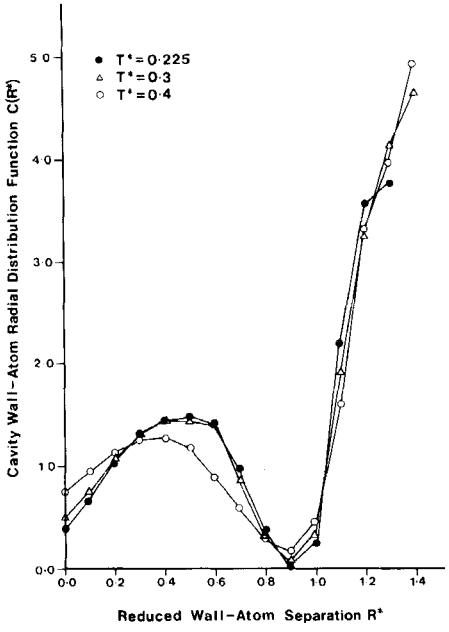

Figure 3B Wall–atom distribution functions for the 13 atom cluster. Notation as for *Figure* 3A.

and -0.5 the probability of finding a particular interior angle is almost uniform. In the liquid phase with pairwise additive potentials a peak at 0.5 is to be expected since equilateral triangles with sides of length equal to the pair separation with the minimum potential energy will be energetically favourable. An atom may take part in more than one such triangle leading to a second peak near -0.5, although this will be much reduced in height compared to that in the solid phase. The plot of $f(\cos\theta)$ in Figure 3C for $T^* = 0.4$ indicates that at this temperature the microcrystal has melted into a liquid phase (Figure 3B clearly shows that this phase is inhomogeneous).

The structural data presented in this section provides no sign of an abrupt phase transition in the 13 atom cluster. Figures 3A, B, C showed a gradual loss of order from high temperature solid to inhomogeneous liquid. The continuous nature of the transition is confirmed in Figure 3D where the value of $f(\cos\theta)$ for $\cos\theta = 0$ is plotted against temperature. At low temperatures ($T^* \leq 0.225$) the value of $f(0)$ is very small as it should be for the icosahedral structure. The fraction of interior angles with $\cos\theta = 0$ increases gradually as the microcrystal becomes more disordered. The transition temperature can only be assigned by reference to the specific heat which displays an unambiguous peak at $T^* = 0.3125 \pm 0.025$. Berry et al [13–15] have shown that the gradual nature of the "melting transition" of metastable clusters in vacuum can be thought of as being due to the gradual mixing of ordered "solid" and disordered "liquid" forms as the temperature increases. An analogous mixing occurs

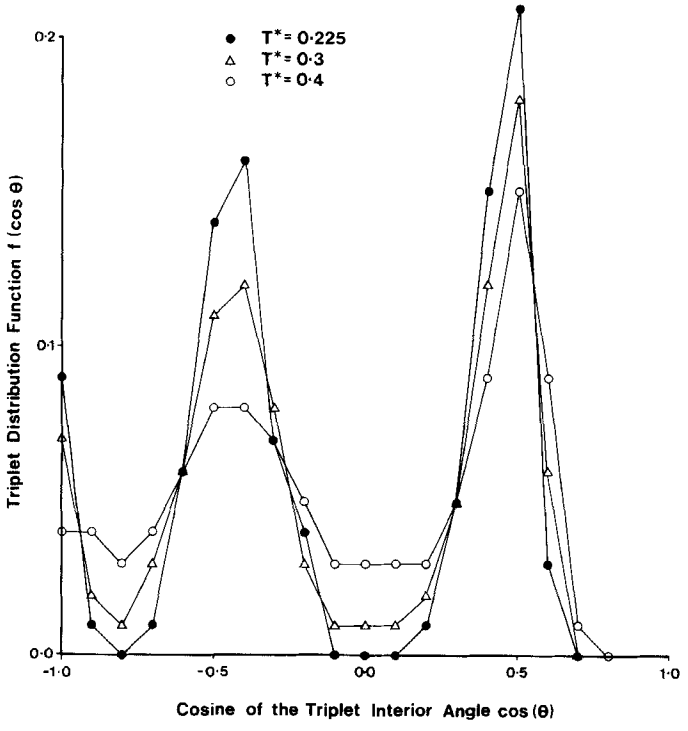

Figure 3C The distribution of interior angles of triplets of atoms in the 13 atom cluster as the microcrystal melts. Only triplets having all pair separations $r^* \leqslant 1.35$ have been counted in order to isolate the nearest neighbour structure. (Two significant figures have been used in plotting $f(\cos\theta)$).

for the case of the present clusters. The gradual variation of $f(0)$ in Figure 3D occurs because it is the average of "solid" configurations with $f(0) \sim 0$ and disordered configurations with $f(0) \neq 0$, the proportion of disordered configurations increasing with temperature. Figure 1C indicates that even the high temperature liquid cluster at $T^* = 0.4$ (well to the right of the specific heat peak in Figure 1B) samples low energies characteristic of clusters at much lower temperatures. A division of the cluster configurations into those associated with high and low energies shows that low energies (eg $U^* = -3.08$) are correlated with solid-like structures and high energies (eg $U^* = -2.46$) with very disordered "liquid" configurations. It is important to note that intermediate energies show intermediate degrees of disorder – the confined clusters considered here are not confined to two distinct states, "solid" and "liquid" but rather to a continuum of more, or less ordered, states.

Figure 3E shows $n(R^*, U^*)$ the mean number of atoms at distances between R^* and $R^* + dR^*$ from the centre of mass for configurations with a potential energy U^* in the range -3.08 ± 0.16 for $T^* = 0.4$ (on the right hand side of the specific heat peak in Figure 1B) and $T^* = 0.275$ (on the left hand side of the peak) at a density $\rho^* = 0.875$ (cavity radius $h^* = 1.52$). The figure indicates that the low energy

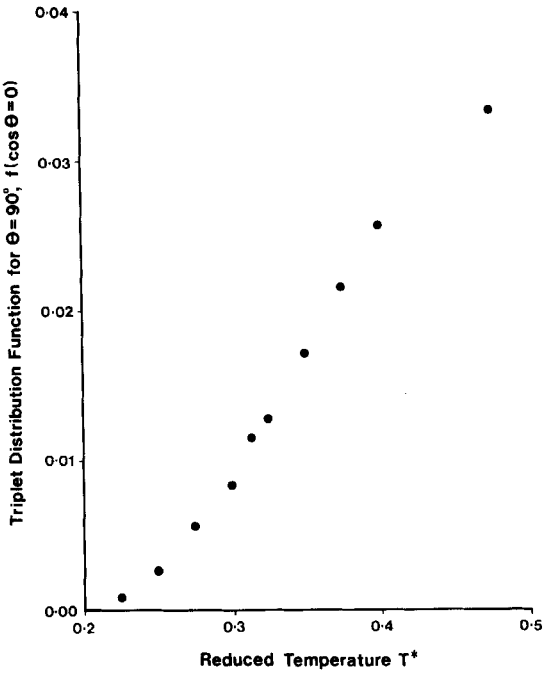

Figure 3D The value of $f(0)$ as a function of temperature through the melting transition of the 13 atom cluster. The continuous change from very low numbers of 90° interior angles ($cos\ \theta = 0$) to approximately what would be expected from a uniform distribution of angles ($f(0) = 0.05$, for 19 bins in the histogram) reflects the continuous nature of the phase transition from a solid icosahedral microcrystal at low temperatures to an inhomogeneous liquid phase at higher temperatures.

configurations are associated with well defined clusters with a central atom and 12 neighbours forming an outer shell. Other structural functions confirm these configurations to be icosahedral, so that even at $T^* = 0.4$, firmly on the "liquid" side of the transition temperature some equilibrium configurations of the system are "solid." The results for a much larger cavity ($\rho^* = 0.1, h^* = 3.14$) are indistinguishable from those displayed in the figure, indicating that the solid structures are uninfluenced by the size of the cavity. At higher energies ($U^* = -2.46 \pm 0.16$), the function $n(R^*, U^*)$ shows much more disordered arrangements (Figure 3F). Larger cavities (e.g. $\rho^* = 0.1, h^* = 3.14$) are now different with a much more disordered or "liquid" like structure for the higher energies than the smaller cavities displayed above.

2.2.2 Larger clusters

In contrast to the 13 atom microcrystal, the 201 atom cluster displays abrupt structural changes on either side of the melting temperature, thus Figure 2A shows an abrupt change in configurational energy on cooling at $T^* = 0.375$ which is reflected in Figure 4A where $g(r^*)$'s for two temperatures are plotted. They represent the pair structure for the 201 atom cluster as it is cooled from $T^* = 0.375$ to $T^* = 0.370$.

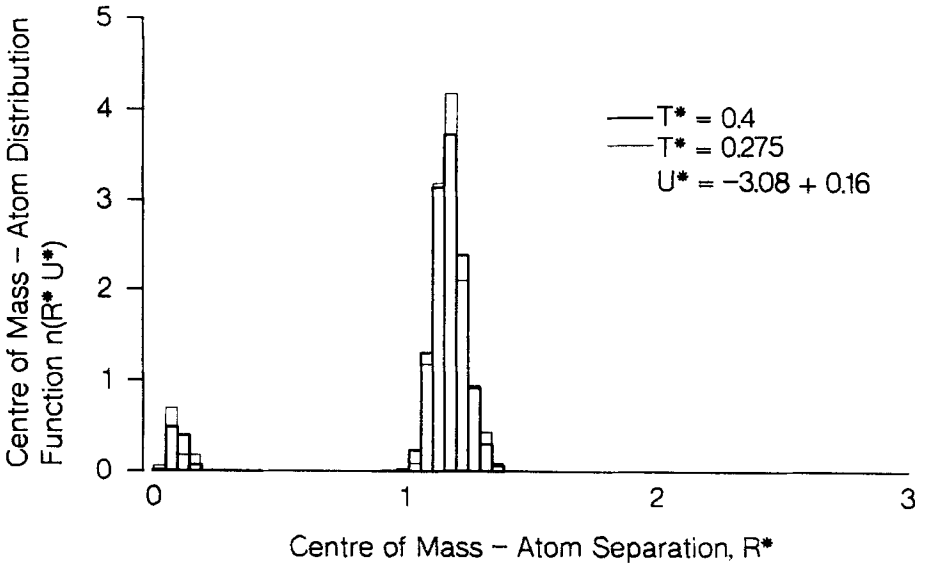

Figure 3E The distribution function $n(R^*, U^*)$ for U^* in the range -3.08 ± 0.16 at $T^* = 0.4$ and 0.275 ($\rho^* = 0.875$ in both cases). Refer to Figure 1C for the corresponding cluster energy distributions.

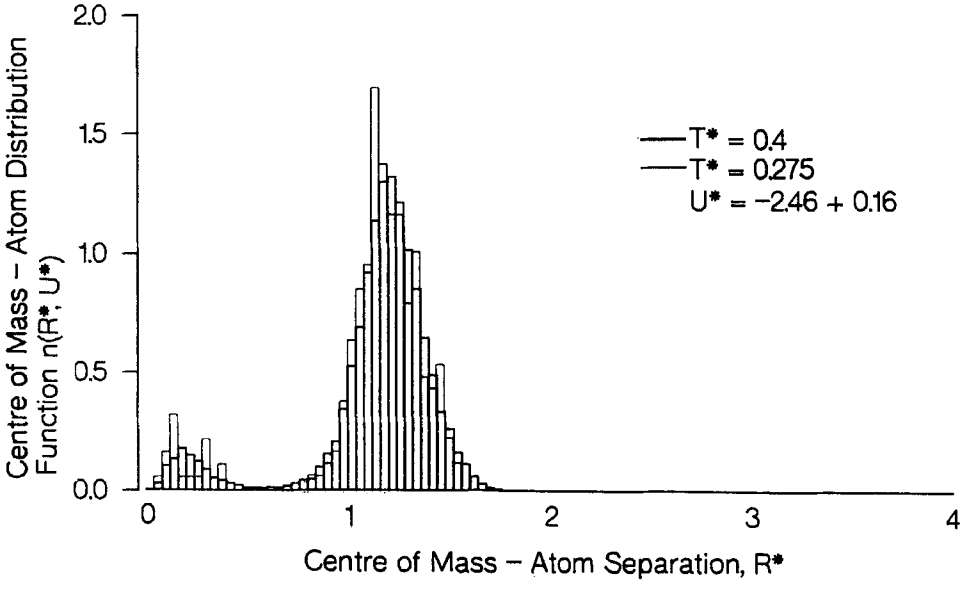

Figure 3F As for Figure 3E except for the high energy configurations, $U^* = -2.46 \pm 0.16$.

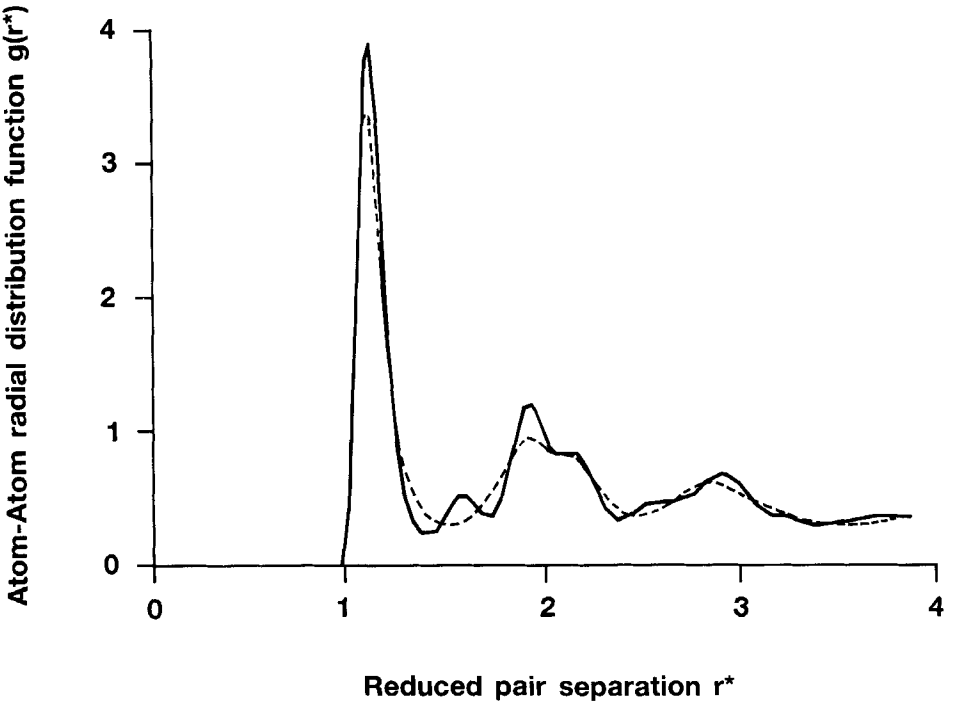

Figure 4A Radial distribution functions for the 201 atom cluster on either side of the freezing transition. The dashed curve represents $g(r^*)$ for $T^* = 0.375$. The full curve represents $g(r^*)$ at $T^* = 0.370$. These results were obtained by slow cooling from a bulk liquid configuration at $T^* = 10.0$.

Two qualitatively different curves are present – a smoothly varying curve ($T^* = 0.375$) with peaks at $r^* = 1.$, 2., 3., – and a more structured curve ($T^* = 0.370$) with peaks at intermediate values of r^* including $r^* = 1.6$. A comparison of the structured curve with the perfect FCC and HCP microcrystal $g(r^*)$s indicate that the microcrystals for $T^* \leq 0.370$ have a structure which is consistent with a temperature broadened close packed arrangement. The sudden reappearance of crystalline ordering on cooling from a liquid configuration in these simulations is in marked contrast to the situation in simulations of bulk liquids with small numbers of particles where, unless special techniques are employed, supercooled liquids or amorphous solids are created on cooling past the freezing point [24]. In order to see whether the close packed ordering was induced by the spherical cavity boundary conditions employed in the microcrystal simulations a liquid configuration at $T^* = 0.375$ was used as the starting point for a simulation in vacuum at $T^* = 0.365$. A short run was sufficient to show the formation of the peak at $r^* = 1.6$ in $g(r^*)$ and the peaks near $r^* = 2.0$. It would appear that the solid structure observed in the present work is not specific to the model cavity employed to constrain the liquid phase.

The changes in three body structure in the core of the microcrystal on freezing are displayed in Figure 4B. The liquid curve (no peak at $cos\theta = 0$) for $T^* = 0.375$,

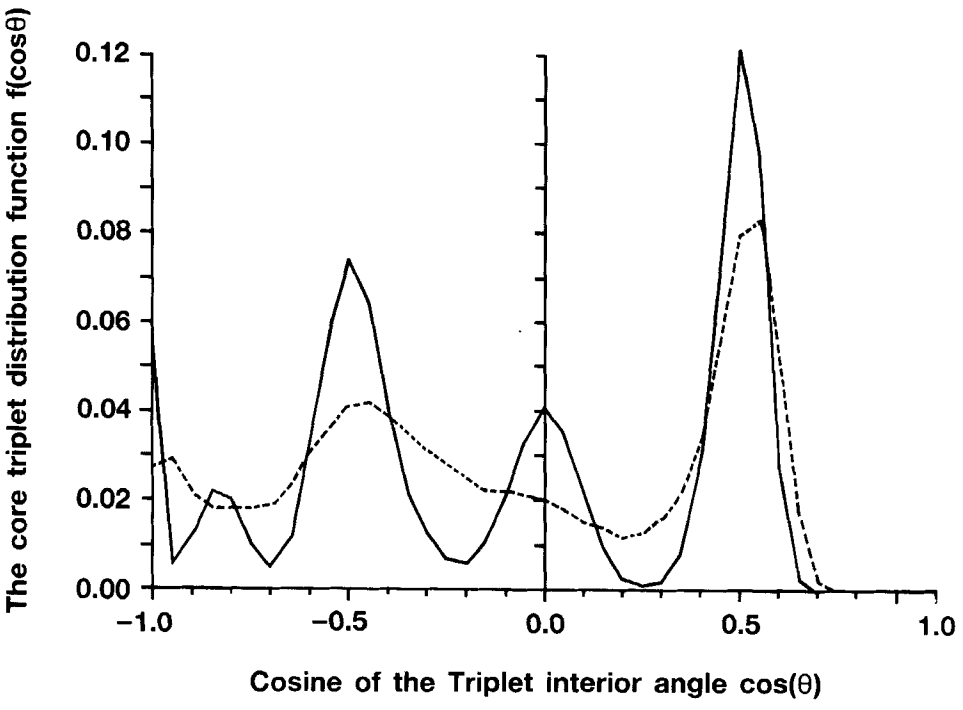

Figure 4B The distribution of interior angles θ of triplets of atoms in the core of the 201 atom cluster before ($T^* = 0.375$, dashed) and after the freezing transition ($T^* = 0.370$, full curve). Only interior angles formed at an atom whose centre is within an atomic diameter of the centre of the cavity are considered and all triplets considered have sides of length smaller than or equal to 1.35.

reducing the temperature to $T^* = 0.370$ leads to a major change in local structure with the appearance of sharp peaks at -1.0, $-.85$, ± 0.5, 0.0. These peaks are consistent with HCP local ordering as discussed in section 2.2.1. The N = 209 cluster displays similar sharp changes in structure on freezing with the formation of strong peaks in $g(r^*)$ and $C(r^*)$ (not shown) in approximately the same positions as for $N = 201$. Figure 4C confirms that the underlying structure is HCP at low temperatures ($T^* = 0.15$) – the extra HCP peak near $cos\theta = -0.33$ is becoming visible. A typical solid configuration is displayed in Figure 4D. All results analysed for the $N = 209$ and 201 clusters are consistent with a freezing transition from an inhomogeneous liquid to an HCP microcrystal. Although the local microcrystal structure is HCP for $N = 201$ and 209 the solid phase in the simulations reported here was not, in the standard notation ABABABAB [26], but in almost all cases, contained a dislocation so that the structure became ABA′CAC with the layer containing the central atom of the cluster indicated by A′ (this stacking sequence is found in zeolites such as afghanite [27]). In this arrangement the central atom sees its nearest neighbours arranged in an FCC structure while these same nearest neighbours will see HCP local ordering. The calculated triplet distribution functions show an FCC structure for the central atom and HCP for its nearest neighbours and the rest of the cluster.

The lattice constant ($\sqrt{2}$ × the mean nearest neighbour distance in the core) de-

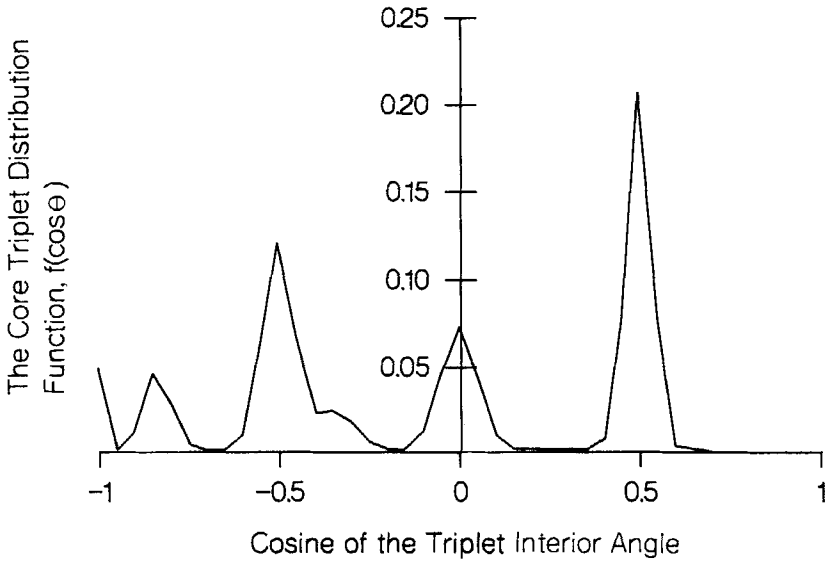

Figure 4C The low temperature ($T^* = 0.15$) 209 atom angular structure in the core region indicating HCP structure (details as for Figure 4B).

creased rapidly with temperature from 5.38 Å at $T^* = 0.38$ to 5.27 Å at $T^* = 0.15$ – a variation almost three times that of bulk argon for the same temperature range [39].

2.3 The Melting Temperature

Briant and Burton [9] report melting temperatures for Lennard-Jones argon microcrystals in vacuum obtained by molecular dynamics (microcanonical ensemble) for $7 \leq N \leq 100$. In this section their results will be used to obtain a simple expression for the melting temperature of a Lennard-Jones microcrystal as a function of size. At the bulk melting temperature ($T_m\{\infty\}$), the chemical potentials in the solid (μ^s), and liquid (μ^l), phases are identical. The presence of a surface can be considered to perturb this bulk transition in a similar fashion to the imposition of an external field. The free energy of the perturbing surface must now be included in the phase equilibrium calculation. If 'S' is the area of the surface of tension of the cluster, here assumed to be the same in both phases (constrained in the same cavity) and γ_s, γ_l are the surface free energies of the solid and liquid phases respectively, then at melting,

$$\mu^s + \Delta\mu = \mu^l, \tag{1}$$

with

$$\Delta\mu = \frac{S\Delta\gamma}{N}, \qquad \Delta\gamma = \gamma_s - \gamma_l.$$

Assuming that the shift in melting temperature, $\Delta T = T_m\{\infty\} - T_m\{N\}$, (where

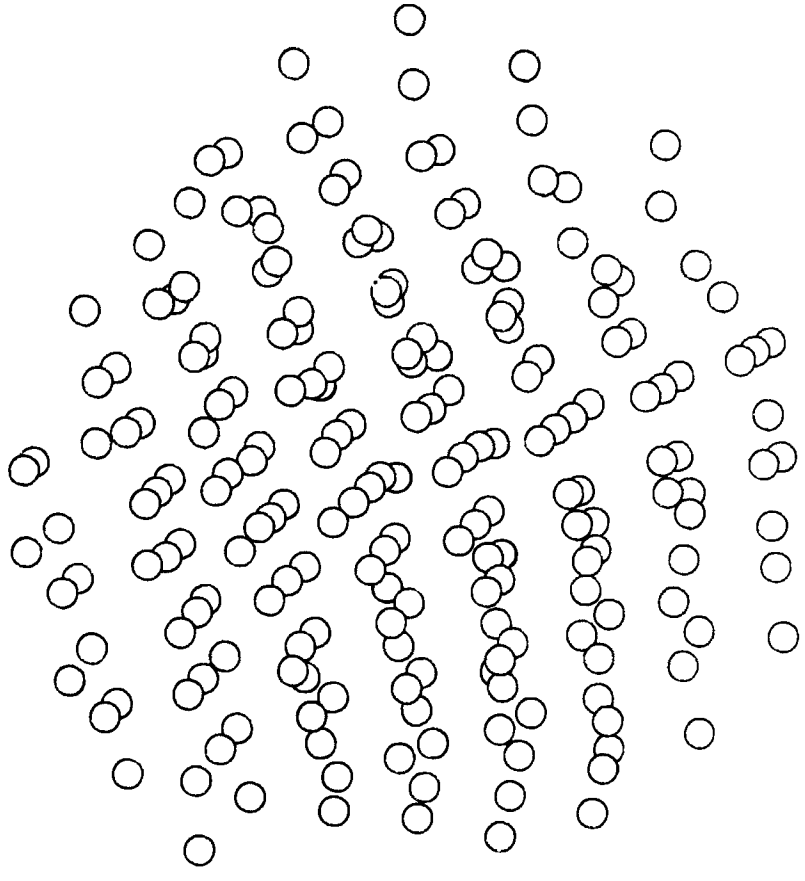

Figure 4D The final configuration from a simulation of 209 Lennard–Jones atoms at $T^* = 0.15$ removed from the hard constraining cavity and run for 10^5 steps. The colour images were produced using CHEMX [42], a reduced atomic diameter has been used in order to display atomic ordering. (See colour plate IV.)

$T_m\{N\}$ is the N atom cluster melting temperature) is proportional to $\Delta\mu$ then:

$$\Delta T^* = \alpha\Delta\gamma^*/N^{1/3}. \quad (2)$$

In writing equation 2, S has been assumed to be proportional to $N^{2/3}$, and α is a constant of proportionality. (This equation is an adaption to the case of microcrystal melting of the expression given by Fisher and Berker [17] for the shift in the ferromagnetic transition at $0K$ of the Ising model due to the presence of a boundary). If $\Delta\gamma^*$ does not depend on N, a straight line dependence of T_m on $N^{1/3}$ (or the cluster radius) is predicted. However, the data of Briant and Burton [9] shown in Table 1 do not support this approximation. The change in $T_m\{N\}$ is rapid at first but then slows considerably. Clearly some account must be taken of the variation of $\Delta\gamma^*$ with cluster size.

From classical thermodynamics, the surface tension of a curved interface is given by the Tolman equation [18]:

Table 1 Melting temperatures for Lennard-Jones microcrystals. N is the number of atoms in the cluster, T_m^*(BB) is the melting temnperature given in Reference 9.

N	T_M^*(BB)	T_M^*(this work)
7	0.167	
13	0.292	0.313 ± 0.025
33	0.317	
55	0.334	
100	0.342	
201		0.3725 ± 0.0025
209		0.385 ± 0.005

$$\gamma = \gamma_\infty - \frac{2\gamma_\infty \delta}{R_s} \tag{3}$$

where γ_∞ is the surface tension of a planar surface, R_s is the radius of the surface of tension, and, R_e the radius of the equimolar dividing surface, $\delta = R_e - R_s$. Assuming $R_s \propto N^{1/3}$ with δ = constant, an approximate form of equation 3 may be obtained which fits the data of Thompson et al [19] for the liquid–vapour surface tension of small Lennard-Jones drops quite well. If this is used as a first approximation for both liquid and solid cluster surface free energies, a tractable expression for $\Delta\gamma^*$;

$$\Delta\gamma^* = \Delta\gamma_\infty^* - \alpha' N^{-1/3}, \tag{4}$$

is obtained, with α' another constant. Equations (2) and (4) give:

$$\Delta T^* = AN^{-1/3} - BN^{-2/3} \tag{5}$$

where A and B are unknown constants.

In order to evaluate A and B a value is required for $T_m^*\{\infty\}$. Since the melting temperature of the bulk is a relatively weak function of pressure and the clusters considered here have either zero or a small applied pressure, the bulk triple point temperature has been employed for $T_m^*\{\infty\}$. Using this value a plot of $N^{1/3}\Delta T^*$ versus $N^{-1/3}$ for $N \leq 100$ using the values of $T_m^*\{N\}$ given in Table 1 is approximately linear except for the smallest clusters ($N \leq 13$). These clusters are essentially all surface and therefore the present arguments could not be expected to apply. A fit of equation 5 to $T_m^*\{33\}$ and $T_m^*\{100\}$ gives:

$$\Delta T^* = 2.46N^{-1/3} - 4.15N^{-2/3} \tag{6}$$

At present, the melting temperature of only two microcrystals with $N > 100$ are known, those for $N = 201$ and $N = 209$ reported in this work. These microcrystals melt at $T_m^*\{201\} = 0.3725$ and $T_m^*\{209\} = 0.385$. Remarkably, equation 6 predicts $T_m^* = 0.38$ for both microcrystals to two significant figures. Figure 5 shows a plot of T_m^* against the number of atoms in a microcrystal, according to equation 6. It is noticeable that even for $N = 10{,}000$, the melting temperature is some 15 per cent below the bulk result. However, the variation of γ with N appears to be important only for $N \leq 2000$. However the Lennard-Jones interaction is relatively short ranged and where longer range interactions (eg dipolar forces) are important these are likely to increase the importance of the surface in larger clusters and further slow the approach to bulk behaviour (see for example, reference 34).

The Tammann temperature, $T = 0.57\ T_m\{\infty\}$, has been defined as a temperature

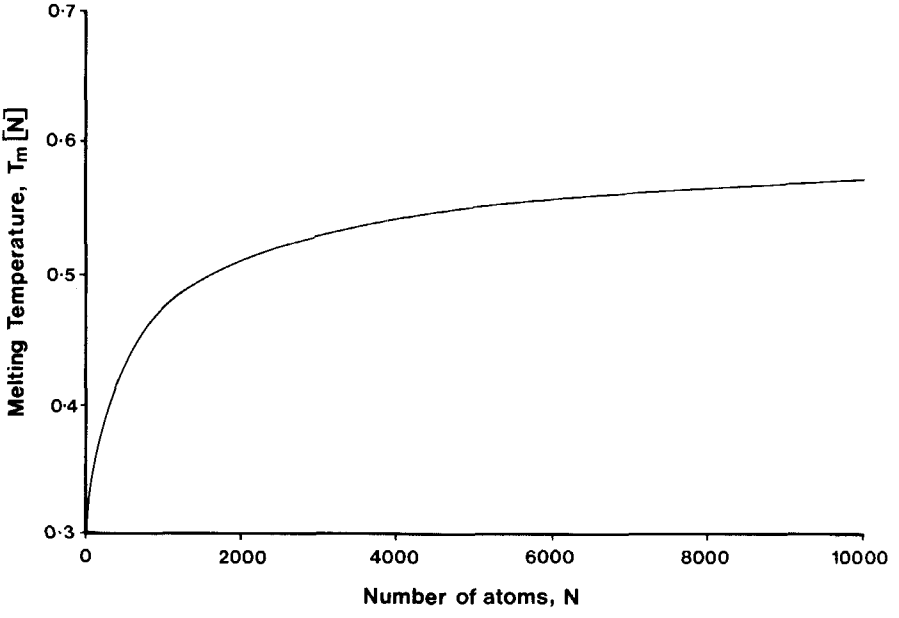

Figure 5 The variation of melting temperature with the number of atoms in a Lennard–Jones cluster {N}, according to equation 6 of the text. For N $\leqslant$ 2000 atoms the value of the melting temperature is controlled by the variation of surface free energy with curvature. The bulk triple point is at $T^*_m\{\infty\} = 0.68 \pm 0.02$ [20].

marking the onset of mobility of lattice atoms or ions [35]. In catalysis, the Tammann temperature is used as a rule of thumb to indicate the temperature at which significant sintering of microcrystals can be expected to occur leading to high surface mobility for the cluster species (see for example the discussion of oxide clusters in reference 36). For the Lennard-Jones systems studied here, this rule is seen to be remarkably accurate with clusters of around two hundred atoms (and smaller) liquid at $T = 0.56\, T_m\{\infty\}$.

For larger clusters the present formula for the melting temperature is consistent with earlier work of Couchman and Jesser [37] and with experimental results for the melting of metal microcrystals. Equation 6 predicts a melting temperature of $T = 0.85\, T_m\{\infty\}$ for clusters of radius 50Å (N = 11,605) and $T = 0.92\, T_m\{\infty\}$ for 100Å (N = 92,842) in good qualitative agreement with experimental results for tin, indium and gold [37]. The similarity between the melting of Lennard-Jones clusters and that of pair potential models of metal clusters is apparent from simulations of the melting of 13 atom copper clusters [41] using the IPS [38] copper pair potential. This very small copper cluster assumed an icosahedral structure in the solid phase and melted via a very smooth transition between reduced temperatures of $T^* = 0.25$ and $T^* = 0.35$. This melting range is similar to that of Figure 1A for the Lennard-Jones potential. Taking the melting temperature to be the mid-point of this range leads to the prediction that such a copper cluster would melt at 618 K ($T^* = 0.3$, $\varepsilon = 2061.7\,K$) compared to the bulk melting temperature of 1356 K.

3. THE APPROACH TO BULK STRUCTURE

The last section has demonstrated significant finite size effects on melting in Lennard-Jones clusters. The solid structure of such clusters is icosahedral for 13 atoms, and HCP for 201 and 209 atoms. Previous work [28] has shown that a range of icosahedral geometries is possible for special "magic" values of N as N increases (eg $N = 13, 55, 147, 309, 561, \ldots$). Some of these isosahedra have been detected in simulations and in argon clusters formed in free jet expansions [29]. More complicated structures of icosahedral symmetry which fill some of the gaps between the magic numbers are also possible [21]. It has been suggested [30] that the approach to the bulk crystal with increasing cluster size is through a series of icosahedral arrangements which merge in some fashion with the bulk FCC structure for N greater than some critical value. This critical N has been put at 800 for argon [30] while a value of 150 has been suggested for nickel [31]. For the special case of the infinite range Lennard-Jones potential the bulk structure is HCP (see references 32 and 33) and as N becomes very large this structure should predominate.

Both the 201 and 209 atom clusters display close packed crystalline structures and showed no signs of icosahedral ordering with and without the confining cavity. Further, truncating the Lennard-Jones potential at $r^* = 1.6$ so that a bulk phase with this potential is unlikely to favour an HCP structure [33] did not change the structure of the 209 atom microcrystal on freezing from the liquid cluster (the melting temperature dropped however). Nor is the choice of FCC or HCP associated with the ability to form closed outer shells of atoms. For $N = 201$ only an FCC structure has a complete shell of 24 atoms while for $N = 209$ a perfect HCP structure provides outermost shells containing 12 and finally just 2 atoms [32]. (Note that the smaller clusters simulated in the present study do not probe the long range part of the potential in the solid phase since they are confined to very small microcrystallites. Their behaviour will be independent of any truncation of the atom-atom potential outside the microcrystal diameter and will be valid for a range of possible Lennard-Jones like potentials).

On the basis of the limited evidence presented here it is possible to speculate that bulk crystal structure has been reached with $N \sim 200$. The prediction of "magic" numbers for the appearance of icosahedra with $N > 200$ remains to be tested for finite temperature Lennard-Jones clusters. Further exploration of the structural transitions with increasing N (> 200) by simulation would be facilitated by the use of a shorter range potential than has been employed here due to the computational cost of including all interactions and of overcoming metastability in the melting region.

4. CONCLUSIONS

Simulation studies show a very large drop in melting temperature for small clusters of atoms to about half that of the bulk material in agreement with the Tammann criterion. There are qualitative differences between the melting of 13 atom clusters and that of 201 and 209 atom clusters, with both the microcrystalline structure and the sharpness of the melting transition being bulk-like for the larger clusters. The 13 atom melting transition conforms to the qualitative picture of finite size effects on first order transitions proposed by Challa et al [8]. A simple formula for the variation of cluster melting temperature with size has been proposed which is in qualitative agreement

with experiment for large clusters of metal atoms which may be useful in extrapolating melting temperatures to much smaller clusters. The reduction in melting temperature for Lennard-Jones clusters containing less than about 2000 atoms is controlled by the variation of surface free energy with cluster radius. The present results imply a very complicated series of changes in microcrystal structure as the number of atoms increases. Icosahedral, HCP and layered close packed structures are possible even for very small clusters.

ACKNOWLEDGEMENT

It is a pleasure to acknowledge useful discussions with Prof R.S. Berry, and the assistance of Dr S. Ramdas and Dr J.P.R.B. Walton in producing Figure 4D. The author wishes to thank BP International plc for agreeing to the publication of this work.

APPENDIX

The details of the simulations reported in the main text are given in this appendix.

Potential Functions

The simulations reported here are for clusters of Lennard-Jones atoms. The choice of Lennard-Jones parameters $\sigma = 3.405\,\text{Å}$ and $\varepsilon/k_B = 119.8K$ where k_B is the Boltzmann constant, gives an approximate model for argon. The Lennard-Jones atoms were confined to spherical cavities of two types – hard cavities in which the atom wall potential U^H_{AW} was a hard sphere potential and soft cavities for which U^S_{AW} was a modified Lennard-Jones potential. If h is the radius of a hard cavity and d is the distance of an atom from the cavity centre then the hard potential has the form:

$$U^H_{AW}(r) = 0 \qquad d < h$$
$$U^H_{AW}(r) = \infty \qquad d \geq h.$$

For the 13 atom cluster $h^* = 1.525$ while for the 201 and 209 atom clusters $h^* = 3.799$ and 3.849 respectively. These values arose from the requirement that both clusters have a mean density of $\rho^* = 0.875$.

In the soft cavity the atoms interact with the wall via a Lennard-Jones potential which has been cut at the minimum of the potential and shifted upwards by the well depth to produce a repulsive interaction energy. In order to create a cavity of effectively the same volume as for the hard cavity, the Lennard-Jones sigma parameter for the atom-wall potential σ_{AW} has been taken to be h, with ε_{AW} kept equal to ε. For the soft cavity, the atom wall potential is:–

$$U^S_{AW} = 4\varepsilon\left[\left(\frac{h}{2h-d}\right)^{12} - \left(\frac{h}{2h-d}\right)^{6}\right] + \varepsilon, \qquad 2h-d < 2^{1/6}h$$
$$= 0, \qquad 2h-d > 2^{1/6}h$$

Algorithms

All simulations of clusters in hard cavities were carried out using the Metropolis Monte Carlo (MC) method of generating configurations of particles in the canonical ensemble. For the soft cavity a modified molecular dynamics procedure which generates configurations at constant temperature producing averages in the isokinetic ensemble (MD) was employed. The details of this method have been discussed elsewhere [see e.g. reference 22]. The Monte Carlo and molecular dynamics simulations give similar thermodynamic properties. For soft cavities only the atom-atom interaction energies are used to calculate the configurational energy.

Equilibration and Production

The Monte Carlo simulations for the 13 atom clusters reported in this paper were started from an FCC microcrystal which then relaxed into an icosahedral form or into an inhomogeneous liquid, depending on the temperature. The molecular dynamics simulations were started at the lowest temperature from an FCC microcrystal after which the starting configuration for each temperature was taken as the final configuration of the previous run in order of increasing temperature. Table A1 contains some of the results. Equilibration took place over $n_e = 192{,}000$ iterations of the entire 13 atom cluster (ie 2.5×10^6 single Monte Carlo moves) after which averages were taken over the production phase of n_p iterations of the entire cluster. For some runs n_p was as high as 1.54×10^6. The molecular dynamics runs were equilibrated for 30,000 steps with production over the following 30,000 steps with a time step of 10 femtoseconds.

Table A2 gives details of the 201 atom simulations in the vicinity of the freezing transition. All the 201 atom simulations were performed using Monte Carlo methods and a hard cavity. n_e and n_p refer to iterations of the entire 201 atom cluster so that, for example, the cluster at $T^* = 0.365$ was equilibrated over approximately 20×10^6 single atom moves. Acceptance ratios were kept to around 20 per cent of the trial

Table A1 Results for the 13 atom clusters. These thermodynamic results are a subset of those plotted in Figures 1A and 1B. P^* is the normal pressure at the cavity wall calculated from the cluster virial [23].

N	'METHOD'	T^*	$-U^*$	C_v^*	P^*	$n_e/10^3$	$n_p/10^3$
13	MC/HC	0.225	3.056	2.1	0.05	192	960
		0.250	2.994	2.6	0.07	192	154
		0.275	2.920	3.1	0.08	192	192
		0.300	2.848	3.5	0.11	192	192
		0.3125	2.802	3.6	0.11	192	770
		0.325	2.761	3.5	0.13	192	192
		0.350	2.676	3.2	0.16	192	1540
		0.375	2.604	2.8	0.21	192	1350
		0.400	2.534	2.4	0.24	192	192
13	MD/SC	0.200	3.07			30	30
		0.250	2.99			30	30
		0.300	2.80			30	30
		0.350	2.63			30	30
		0.400	2.53			30	30
		0.450	2.42			30	30

Table A2 Results for the freezing transition of the 201 atom cluster. This series of simulations was started from a 201 atom configuration removed from a simulation of a bulk Lennard-Jones liquid at $T^* = 10$ and $\rho^* = 0.875$. The 201 atoms were then cooled in stages in the cavity to $T^* = 0.4$. n_c and n_p refer to the number of *complete* iterations of the 201 atom cluster.

T^*	$-U^*$ (± 0.02)	P^*	C_v^*	$n_c/10^3$	$n_p/10^3$
0.400	5.03	0.20	2.8	200	100
0.385	5.07	0.19	2.8	200	100
0.375	5.10	0.17	3.4	200	100
0.370	5.32	0.13	3.7	100	100
0.365	5.35	0.10	3.5	200	100
0.350	5.40	0.09	3.3	800	100

Table A3 Results for the freezing transition of the 209 atom cluster.

T^*	$-U^*$	P^*	C_v^*	$n_c/10^3$	$n_p/10^3$
0.420	5.012	0.23	2.64	100	200
0.400	5.058	0.20	2.53	100	300
0.380	5.330	0.12	3.82	100	300
0.350	5.434	0.09	3.22	100	200
0.300	5.595	0.04	2.30	100	100
0.250	0.698	0.02	2.08	100	100

configurations. These long runs were crucial in identifying the sharp nature of the 201 atom melting transition. For shorter runs metastable states were encountered with melting apparently taking place more gradually at significantly higher temperatures. Table A3 gives some results for $N = 209$.

References

[1] J. Feder, K.C. Russell, J. Lothe and G.M. Pound, "Homogeneous nucleation and growth of droplets in vapour" *Advan. Phys.* **15** (1966) 111.

[2] M.R. Hoare and P. Pal, Physical cluster mechanics. Statics and energy surfaces for monatomic systems" *Advan. Phys.* **20** (1971) 161.

[3] J.J. Burton, "Structure and properties of microcrystalline catalysts" *Cat. Rev. Eng. Sci.* **9** (1974) 209.

[4] J.G. Dash, *"Films on solid surfaces,"* Academic Press, New York (1975).

[5] P.W. Winter and D.A. MacInnes, "An analysis of the thermodynamics of gas atoms in very small bubbles" *J. Nuc. Mat.* **114** (1983) 7.

[6] L.R. Foulkner, "Chemical microstructures on electrodes" *C. and E. News*, February **27** (1984) 28.

[7] O.G. Mouritsen, *"Computer studies of phase transitions and critical phenomena,"* Springer-Verlag, (1984).

[8] M.S.S. Challa, D.P. Landau and K. Binder, "Finite-size effects at temperature-driven first-order transitions" *Phys. Rev. B.* **34** (1986) 1841.

[9] C.L. Briant and J.J. Burton, "Molecular dynamics study of the structure and thermodynamic properties of argon microclusters" *J. Chem. Phys.* **63** (1975) 2045.

[10] J.B. Kaelberer and R.D. Etters, "Phase transitions in small clusters of atoms" *J. Chem. Phys.* **66** (1977) 3233.

[11] V.V. Nauchetel and A.J. Pertsin, "A Monte Carlo study of the structure and thermodynamic behaviour of small Lennard-Jones clusters" *Molec. Phys.* **40** (1980) 1341.

[12] N. Quirke and P. Sheng, "The melting behaviour of small clusters of atoms" *Chem. Phys. Letts.* **100** (1984) 63.

[13] R.S. Berry, J. Jellinek and G. Natanson, "Unequal freezing and melting temperatures for clusters" *Chem. Phys. Letts.* **107** (1984) 227; "Melting of clusters and melting" *Phys. Rev. A.* **30** (1984) 919.

[14] J. Jellinek, T.L. Beck, R.S. Berry, "Solid-liquid phase changes in simulated isoenergetic Ar_{13}" *J. Chem. Phys.* **84** (1986) 2783.
[15] H.L. Davis, J. Jellinek, R.S. Berry, "Melting and freezing in isothermal Ar_{13} clusters" *J. Chem. Phys.* (Submitted).
[16] J.Q. Broughton, L.V. Woodcock, "A molecular dynamics study of surface melting" *J. Phys.* **c 11** (1978) 2743.
[17] M.E. Fisher and A. Nihat Berker, "Scaling for first-order phase transitions in thermodynamic and finite systems" *Phys. Rev. B.* **26** (1982) 2507.
[18] J.S. Rowlinson and B. Widom, *Molecular theory of capillarity,"* Clarendon, Oxford (1982).
[19] S.M. Thompson, K.B. Gubbins, J.P.R.B. Walton, R.A.R. Chantry and J.S. Rowlinson, "A molecular dynamics study of liquid drops" *J. Chem. Phys.* **81** (1984) 530.
[20] J.P. Hansen and L. Verlet, "Phase transitions of the Lennard-Jones system" *Phys. Rev.* **184** (1969) 151.
[21] M.R. Hoare, "Structure and dynamics of simple microclusters" *Adv. in Chem. Phys.* **40** (1979) 49.
[22] D. Fincham, N. Quirke and D.J. Tildesley, "Computer simulation of molecular liquid mixtures. I. A diatomic Lennard-Jones model mixture for CO_2/C_2H_6" *J. Chem. Phys.* **84** (1986) 4535.
[23] J.G. Powles, G. Rickayzen and M.L. Williams, "A curious result concerning the Clausius Virial" *J. Chem. Phys.* **83** (1985) 293.
[24] C.A. Angell, J.H.R. Clarke and L.V. Woodcock, "Interaction potentials and class formation; a survey of computer experiments" *Adv. in Chem. Phys.* **5** (1981) 397.
[25] A.R. Ubbelhode, *"Melting of crystal structure,"* Clarendon, Oxford (1965).
[26] C. Kittel, *"Introduction to solid state physics,"* J. Wiley and Sons, London (1976).
[27] G.R. Millward, S. Ramdas and J.K. Thomas, "On the direct imaging of offretite, cancrinite, chabazite and other related ABC-6 zeolites and their intergrowths" *Proc. Roy. Soc. London Ser.* **A 399** (1985) 57.
[28] A.L. Mackay, "A dense non-crystallographic packing of equal spheres" *Acta. Cryst.* **15** (1962) 916.
[29] I.A. Harris, R.S. Kidwell and J.A. Northby, "Structure of charged argon cluster formed in a free jet expansion" *Phys. Rev. Letts.* **53** (1984) 2390.
[30] J. Farges, M.F. de Feraudy, B. Raoult and G. Torchet, "Non-crystalline structure of argon clusters. I. Polyicosahedral structure of Ar_N clusters, $20 < N < 50$" *Surface Science* **106** (1981) 95.
[31] M.B. Gordon, F. Cyrot-Lackmann and M.C. Mesjonqueres, "Relaxation and stability of small transition metal particles" *Surface Science* **80** (1979) 159.
[32] J.O. Hirschfelder, C.F. Curtis and R.B. Bird, *"Molecular theory of gases and liquids,"*J. Wiley and Sons, New York (1954). See Table 13.9.
[33] R.A. La Violette and F.H. Stillinger, "Multidimensional geometric aspects of the solid-liquid transition in simple substances" *J. Chem. Phys.* **83** (1985) 4079.
[34] A.P. Shreve, J.P.R.B. Walton and K.E. Gubbins "Liquid drops of polar molecules" *J. Chem. Phys.* **85** (1986) 2178.
[35] A.L.G. Rees, *"Chemistry of defect solid state,"* Methuen, London (1954).
[36] W. Curtis Conner, JR, G.M. Pajonk and S.J. Teichner, "Spillover of sorbed species *"advances in catalysis"* **34** (1986) 1.
[37] P.R. Couchman, W.A. Jesser, "Thermodynamic theory of size dependence of melting temperatures in metals" *Nature,* **269** (1977) 481.
[38] K.W. Ingle, K.C. Perrin and H.R. Schober "Interstitial clusters in FCC metals" *J. Phys. F.* **11** (1981) 1161.
[39] B.L. Smith, "Inert gas crystals" *Contemp. Phys.* **11** (1970) 125.
[40] P. Sheng, R.W. Cohen and J.R. Schrieffer, "Melting transition of small molecular clusters" *J. Phys. C.* **14** (1981) 1565.
[41] N. Quirke, Unpublished results.
[42] CHEMX Distributed by Chemical Design Limited, Oxford, UK.